Materials Today Bio 16 (2022) 100425

Contents lists available at ScienceDirect

Materials Today Bio

journal homepage: www.journals.elsevier.com/materials-today-bio

A tannic acid doped hydrogel with small extracellular vesicles derived from mesenchymal stem cells promotes spinal cord repair by regulating reactive oxygen species microenvironment

Zhong Liu [a,1], Song Guo [a,1], Lanlan Dong [b,1], Peipei Wu [c], Kewei Li [a], Xinhua Li [a], Xiang Li [b,**], Hui Qian [c,d,***], Qiang Fu [a,*]

[a] Department of Orthopedics, Shanghai General Hospital, Shanghai Jiao Tong University School of Medicine, Shanghai, 200080, PR China
[b] School of Mechanical Engineering, Shanghai Jiao Tong University, State Key Laboratory of Mechanical System and Vibration, Shanghai, 200240, PR China
[c] Key Laboratory of Laboratory Medicine of Jiangsu Province, School of Medicine, Jiangsu University, Zhenjiang, 212013, PR China
[d] NHC Key Laboratory of Medical Embryogenesis and Developmental Molecular Biology & Shanghai Key Laboratory of Embryo and Reproduction Engineering, Shanghai, 200040, PR China

ARTICLE INFO

Keywords:
Spinal cord injury
Tannic acid
Hydrogel
Small extracellular vesicle
Mesenchymal stem cell
Reactive oxygen species

ABSTRACT

Spinal cord injury (SCI) is a serious disease of the central nervous system that is associated with a poor prognosis; furthermore, existing clinical treatments cannot restore nerve function in an effective manner. Inflammatory responses and the increased production of reactive oxygen species (ROS) in the microenvironment of the lesion are major obstacles that inhibit the recovery of SCI. Small extracellular vesicles (sEVs), derived from mesenchymal stem cells, are suitable options for cell-free therapy and have been shown to exert therapeutic effects in SCI, thus providing a potential strategy for microenvironment regulation. However, the effective retention, controlled release, and integration of small extracellular vesicles into injured spinal cord tissue are still a major challenge. Herein, we fabricated an N-acryloyl glycinamide/gelatin methacrylate/Laponite/Tannic acid (NAGA/GelMA/LPN/TA, NGL/T) hydrogel with sustainable sEV release (sEVs-NGL/T) to promote the recovery of motor function after SCI. The newly developed functional sEVs-NGL/T hydrogel exhibited excellent antioxidant properties in an H_2O_2-simulated peroxidative microenvironment *in vitro*. Implantation of the functional sEVs-NGL/T hydrogel *in vivo* could encapsulate sEVs, exhibiting efficient retention and the sustained release of sEVs, thereby synergistically inducing significant restoration of motor function and urinary tissue preservation. These positive effects can be attributed to the effective mitigation of the inflammatory and ROS microenvironment. Therefore, sEVs-NGL/T therapy provides a promising strategy for the sEV-based therapy in the treatment of SCI by comprehensively regulating the pathological microenvironment.

1. Introduction

Spinal cord injury (SCI) leads to severe neurological dysfunction including paralysis, incontinence, and chronic pain; these conditions create a significant burden on patients, their family, and wider society [1]. The pathophysiology of SCI is characterized by an original primary injury and a subsequent secondary injury that can be treated. Urgent surgical decompression combined with corticosteroid treatment has been used extensively to alleviate secondary SCI and aims to rescue nerve function [2,3]. However, the overall treatment outcomes for patients

Abbreviations: SCI, spinal cord injury; ROS, reactive oxygen species; sEVs, small extracellular vesicles; NGL/T, N-acryloyl glycinamide/gelatinmethacrylate/Laponite/Tannic acid; HucMSCs, Human umbilical cord mesenchymal stem cells; GFAP, glial fibrillary acidic protein; ChAT, choline acetyl transferase; NF, neurofilament; 4-HNE, 4-hydroxynonenal; 8-OHdG, 8-hydroxy-2′-deoxyguanosine.

* Corresponding author. NO.85 Wujin Road, Shanghai, 200080, PR China.
** Corresponding author. NO.800 Dongchuan Road, Shanghai, 200240, PR China.
*** Corresponding author. NO.301 Xuefu Road, Zhenjiang, 212013, PR China.
E-mail addresses: xiangliwj@sjtu.edu.cn (X. Li), lstmmmlst@163.com (H. Qian), fuqiangtj2020@163.com (Q. Fu).
[1] These authors contributed equally to this work.

https://doi.org/10.1016/j.mtbio.2022.100425
Received 31 March 2022; Received in revised form 20 July 2022; Accepted 9 September 2022
Available online 16 September 2022

with SCI remain poor. There is an urgent need to identify the mechanisms responsible for secondary SCI in order to identify appropriate therapeutic targets at the molecular level.

Secondary spinal cord injuries, such as electrolyte abnormalities and the release of reactive oxygen species (ROS) and excitatory amino acids, cause ischemia, edema, cell necrosis, and apoptosis at the injury site [4,5]. Of these, oxidative stress induced by free radicals can result in damage to spinal neurons, glia, and microvascular cells; therefore, these deleterious conditions are considered hallmarks of the pathophysiology of secondary SCI [6]. Increased levels of ROS have been reported in patients with SCI patients along with significant reductions in antioxidants [7]. In addition, oxidative stress was shown to activate neutrophils to synthesize proinflammatory cytokines, which then played detrimental roles in secondary SCI [8]. Therefore, targeting the inflammatory response and the inhibition of oxidative stress could potentially be an effective therapeutic intervention for secondary SCI. Previous studies have shown that the suppression of triggering receptor expressed on myeloid cells 1 (TREM1) expression in a mouse model significantly reduced the levels of oxidative stress and improved locomotor function along with mechanical and thermal hypersensitivity in mouse hind paws after SCI [9]. Other studies have also shown that antioxidant therapies achieved certain levels of neuroprotection in animal models but only led to limited improvements in human clinical studies [10]. Therefore, there is a clear need to investigate new antioxidant treatments to improve neurological function after SCI.

Tannic acid (TA), as a cross-linker polyphenol, is widely found in many plants and has been used in many biomedical products because of its antioxidant, anti-inflammatory, and antibacterial properties [11]. Several studies have demonstrated the protective effects of TA against injury, with particular emphasis on attenuating the inflammatory response, ameliorating oxidative damage and improving antibacterial activity [12,13]. However, an important issue in the systemic application of TA is that it remains difficult for TA to reach neural tissue in sufficient concentrations and in a biologically active form; these limitations have impeded the clinical development of TA as a potential therapeutic agent. Herein, we established a three-dimensional (3D) biocompatible hydrogel by using TA and gelatin methacrylate (GelMA) to provide relatively high antioxidant and anti-inflammatory abilities to reduce the severe adverse effects of systemic medication. In addition, it has been shown that the 3D structure of porous nanomaterials existing in a hydrogel play a vital role in cellular attachment and the guidance of neurite orientation to enhance neural proliferation and axonal outgrowth [14,15].

In recent years, mesenchymal stem cell-derived small extracellular vesicles (MSC-sEVs) have attracted much attention in SCI therapy. Small extracellular vesicles (sEVs) are extracellular nanovesicles secreted by various cell types with low immunogenicity and nanometer size, allowing them to cross the brain–spinal cord barrier (BSCB) to exert significant therapeutic effects in SCI [16]. Several studies have confirmed the neuroprotective effects of MSC-sEVs against SCI, which have been mainly attributed to the neurotrophic, anti-oxidative, anti-inflammatory, and anti-apoptotic effects of MSC-sEVs [17,18]. These findings indicated the significant potential of MSC-sEVs as a cell-free factor for SCI therapy. However, the systemic application of MSC-sEVs cannot target the injured site directly to realize sustained release, thus creating a major limitation to their use in this context [19]. In addition, unconjugated or free MSC-sEVs at the injured site cannot be retained for long periods [20]. Therefore, it is critical that we develop a biomaterial vehicle that can serve as a sustained release carrier for MSC-sEVs. Herein, we fabricated a sEVs-N-acryloyl glycinamide/gelatin methacrylate/Laponite/TA (sEVs-NAGA/GelMA/LPN/TA, sEVs-NGL/T) functional hydrogel that exhibits excellent antioxidant and anti-inflammatory properties. The sEVs-NGL/T functional hydrogel, which supports local, sustainable, and stable delivery of sEVs, was designed for SCI treatment to comprehensively mitigate the SCI microenvironment. We observed a significant restoration in motor function, nerve tissue repair, and urinary tissue preservation following implantation therapy. These positive effects could be attributed to the effective mitigation of the ROS microenvironment and inhibiting the release of pro-inflammatory cytokines, including tumor necrosis factor α (TNF-α), interleukin (IL)-6, and IL-1β.

2. Materials and methods

2.1. Hydrogel preparation and physicochemical characterization

2.1.1. Materials

2-hydroxy-2-methyl-1-phenyl-1-propanone (Irgacure 1173, 98%) was purchased from Sigma-Aldrich (St. Louis, MO, USA), and Laponite XLG was purchased from BYK Additives and Instruments (Wesel, Germany). N-acryloyl glycinamide (NAGA) was purchased from Zhengzhou Alfa Chemical Co., Ltd (Zhengzhou, China). GelMa, TA, and 1,1-Diphenyl-2-picrylhydrazyl (DPPH) were purchased from Aladdin Co., Ltd (Shanghai, China).

2.1.2. Preparation of NGL/T hydrogels

First, 25% w/v NAGA, 2% w/v Laponite, and 5% w/v GelMA were dissolved in deionized water at 37 °C for 30 min. Then, 1% wt of the photo-initiator Irgacure 1173 (relative to the total weight of the monomers) was dissolved in the NAGA/GelMA/Laponite solution. After complete dissolution, the mixture was cast into plastic molds and crosslinked for 40 min. The hydrogel formed was then immersed in TA solution at a concentration of 5% w/v for 24 h to obtain the NGL/T hydrogels.

2.1.3. Microstructure

The morphology of the hydrogels was observed via scanning electron microscopy (SEM; Merlin FE-SEM; Carl Zeiss AG, Jena, Germany).

2.1.4. Swelling test

Crosslinked cylinder samples (n = 3), with a diameter of 10 mm and a height of 5 mm, were immersed in phosphate-buffered saline (PBS) at 37 °C for 48 h. Prior to weighing, the surface water of the hydrogel was removed gently with filter paper, and the swollen hydrogel was weighed. The swelling ratio was calculated using the following formula:

$$\text{Swelling ratio} = \frac{W_s - W_d}{W_d} \times 100\ \% \quad ,$$

in which W_d is the dry weight of the hydrogel and W_s is the swollen weight of the hydrogel.

2.1.5. Degradation testing

Crosslinked cylindrical samples (n = 3) were prepared to measure degradation. Each sample was weighed and incubated in PBS at 37 °C. The samples were retrieved at the given time points (days 1, 2, 3, 5, 7, 10, 14, 21, 28, 35, 42, 56, 70). The entire supernatant was removed from each dish and the remaining hydrogel was weighed. The following formula was used to calculate the degradation ratio of the hydrogels:

$$\text{Weight Remaining} = \frac{W_t}{W_0} \times 100\% \quad ,$$

in which W_0 is the initial weight of the sample and W_t is the weight of the sample at any given time.

2.2. Cell isolation and culture

Human umbilical cord samples were collected during cesarean section procedures under aseptic surgical conditions. The use of human umbilical cord samples was approved by the ethics committee of Jiangsu University, and written informed consent was obtained before clinical sampling. Human umbilical cord mesenchymal stem cells (HucMSCs) were isolated and characterized. In brief, fresh human umbilical cord tissues were collected from the Fourth People's Hospital Affiliated to Jiangsu University and cut into 1–3 mm^3 tissue pieces within 5 h of

collection. HucMSCs were then cultured in minimal essential medium alpha (MEM-α) containing 10% fetal bovine serum (FBS; Thermo Fisher Scientific, Waltham, MA, USA), 100 U/ml penicillin, and 100 mg/mL streptomycin at 37 °C with 5% CO_2. Cells from passages 3–6 were used for subsequent experiments. PC12 cells were purchased from the Shanghai Cell Bank at the Chinese Academy of Sciences and maintained in Dulbecco's modified Eagle medium (DMEM; Thermo Fisher Scientific) supplemented with 10% FBS in a humidified atmosphere containing 5% CO_2 at 37 °C.

2.3. hucMSCs characterization

2.3.1. Flow cytometry analysis of hucMSCs

To test the multipotency of hucMSCs, cells from passage 3 were cultured in MEM-α containing 10% FBS. Then, an appropriate number of cells were digested, and the cells were re-suspended in PBS to adjust the concentration to 3×10^6 cells/ml. Next, the cells were incubated with several antibodies: purified anti-human CD105, purified anti-human CD29, purified anti-human CD73, purified anti-human CD14, purified anti-human CD11b, and purified anti-human CD45 (all from Cyagen, Santa Clara, USA) and, finally, analyzed by flow cytometry.

2.3.2. The induction of osteogenic and adipogenic differentiation in hucMSCs

HucMSCs from passage 4 were seeded in 12- or 6-well plates and cultured in osteogenic (Cyagen, Santa Clara, USA) and adipogenic differentiation media (Cyagen, Santa Clara, USA) for 21 days. Subsequently, the differentiated cells were fixed in 4% paraformaldehyde (PFA), and adipogenic differentiation was detected by staining lipid droplets with Oil Red O (Cyagen, Santa Clara, USA); mineralization was detected by staining with Alizarin Red (Cyagen, Santa Clara, USA).

2.4. Isolation and identification of sEVs

2.4.1. Isolation of sEVs secreted by hucMSCs

sEVs were isolated and purified by differential ultracentrifugation, as described previously [21]. In brief, hucMSCs were cultured in MEM-α containing 10% sEV-free FBS for 48 h. Next, hucMSCs from passages 3 to 8 were cultured so that we could collect the culture supernatant. Subsequently, sEVs were purified and collected from the conditioned medium. First, the supernatants were centrifuged at 500×*g* for 10 min and 2000×*g* for 10 min at 4 °C to remove dead cells and cell debris. Then, supernatants were centrifuged at 4 °C and 10,000×*g* for 30 min to remove organelles. Subsequently, the supernatants were transferred to a 100-kDa molecular wight cut-off ultrafiltration centrifuge tube (UFC910008; MilliporeSigma, Burlington, MA, USA) and centrifuged at 2000×*g* for 30 min. Next, the concentrated solution from the upper tube was collected for ultracentrifugation at 100,000×*g* for 70 min at 4 °C to pellet the hucMSCs-sEVs. Then, we used PBS to resuspend the sEV pellet and centrifuged again at 100,000×*g* for 70 min. Finally, the pelleted sEVs were resuspended in PBS. The purified sEVs were collected and subjected to filtration through a 0.22-μm pore filter (MilliporeSigma) and the solution was stored in a −80 °C freezer for further analysis or used immediately for experiments.

2.4.2. Nanoparticle tracking analysis

The sizes and concentrations of sEVs were detected by nanoparticle tracking analysis (NTA; NanoSight, Amesbury, UK). sEVs were first prediluted in PBS (1:2000) and then injected into the sample carrier cell. NTA measurement was performed at 11 positions.

2.4.3. Transmission electron microscopy

Transmission electron microscopy (TEM) was used to evaluate the morphology of the isolated sEVs. In brief, a sample of the sEV suspension was loaded onto copper mesh grids and incubated for 15 min. The sEVs were then negatively stained with 3% (w/v) phosphotungstic acid for 5 min. Subsequently, the excess solution on the grid was removed by filter paper and dried at room temperature. Finally, the sample was observed by TEM (Tecnai 12; FEI, Hillsboro, OR, USA).

2.4.4. Western blotting

Western blotting was performed to assess the presence of typical sEV markers (CD81, TGS101, and Alix) and the absence of calnexin expression. Cells and sEVs were successively lysed with radioimmunoprecipitation assay (RIPA) buffer. The protein concentration was then determined using a bicinchoninic acid (BCA) assay kit (Beyotime, Shanghai, China). Then, 5 × sodium dodecyl sulfate loading buffer was added into the preparations as described above. The samples were then denatured by boiling for 10 min and loaded onto 12% sodium dodecyl sulfate-polyacrylamide gel electrophoresis gels. After electrophoresis, proteins were transferred to 0.22-μm polyvinylidene fluoride membranes for 1 h. The polyvinylidene fluoride membranes were then blocked for 2 h at room temperature with blocking buffer and incubated overnight with primary antibodies (1:1000) at 4 °C, including CD81 (ab79559; Abcam, Cambridge, UK), Tgs101 (ab125011; Abcam), Alix (ab117600; Abcam), calnexin (2679; Cell Signaling Technology, Danvers, MA, USA). The following morning, the membranes were washed three times with tris-buffered saline with Tween 20 (10 min per wash) and then incubated for 1 h with secondary antibodies (1:2000) at room temperature. Blots were then detected by enhanced chemiluminescence.

2.5. Preparation of sEVs- NGL/T implants

The lyophilized NGL/T hydrogel was fully swelled in PBS, exposed to UV overnight, and then washed with 70% ethanol and PBS for sterilization. The hucMSC-derived sEVs (1000 μg) were suspended in PBS, and the suspension of sEVs was pipetted in full into the hydrogel. The sEV-encapsulated NGL/T hydrogel was then incubated at 37 °C for 1 h and at 4 °C for 24 h to prepare the sEVs- NGL/T implant.

2.6. Release profile of sEVs from NGL/T hydrogel

To investigate the release behavior of sEVs from the NGL/T hydrogel, sEVs- NGL/T composites were prepared and washed with PBS to remove free sEVs. The composites were incubated in 1 mL of PBS *in vitro*. At predetermined time intervals, the 500-μL supernatant was collected and replaced with an equal volume of fresh medium. The collected samples were then analyzed by BCA assays to determine the amount of free sEVs in the supernatant. The cumulative and daily release profiles over time were calculated and plotted.

2.7. Evaluation of sEVs adhesion and distribution in NGL/T hydrogel

The adherence of sEVs in the NGL/T hydrogel were observed by laser scanning confocal microscopy. Firstly, DiI-labelled sEVs were encapsulated in the NGL/T hydrogel and allowed to adhere to prepare sEVs-NGL/T. The sEVs-NGL/T were then observed by laser scanning confocal microscopy with z-stack scanning to detect DiI signals. The results were three-dimensionally remodeled, and the spatial distribution of sEVs along the z-axis was analyzed.

2.8. Quantification and Dil staining assay

The protein content of sEVs was determined with a BCA assay kit by measuring absorbance at 562 nm. A DiI kit (SLB6089; Sigma Aldrich, St. Louis, MO, USA) was used to label sEVs according to the manufacturer's protocol. In brief, sEVs were incubated with DiI dye solution for 1 h at 37 °C in the dark. Labelled sEVs were obtained after centrifugation at 100,000×*g* for 70 min and resuspended in PBS. We used DiI-labelled sEVs to prepare DiI-sEVs-NGL/T hydrogel, according to the method described above. PC12 cells were incubated with DiI-sEVs-NGL/T hydrogels in a 24-well plate for 24 h. Subsequently, the cells were

washed with PBS, fixed with 4% PFA, and the nuclei were stained with Hoechst 33342 (Sigma Aldrich) for 10 min. Images were visualized by confocal microscopy (GE Healthcare, Chicago, IL, USA).

2.9. In vitro antioxidant activity assay

2.9.1. DPPH radical scavenging assay

A fresh solution of DPPH/ethanol (40 μg/mL) was used for the antioxidant assay. The NGL and NGL/T hydrogels were immersed in 5 mL of DPPH solution and allowed to react for 30 min. The absorbance at 517 nm was measured using an ultraviolet–visible spectrophotometer (Evolution 300; Thermo Fisher Scientific). The free radical-scavenging rate was calculated using the following formula:

$$\text{Inhibition}\% = \frac{A_0 - A}{A_0} \times 100 \quad ,$$

where A_0 is the absorbance of the DPPH solution and A is the absorbance of the hydrogel mixed with the above solution.

2.9.2. Hydrogen peroxide assay

To evaluate the antioxidant function of the NGL/T hydrogel, the controls and functional hydrogels were immersed in cell culture medium. After hydrogel swelling, the medium was replaced by a peroxidative medium containing 100-μM H_2O_2. The concentration of H_2O_2 in the medium was detected after incubation for 1 h with a hydrogen peroxide assay kit (Beyotime, Shanghai, China) in accordance with the manufacturer's protocol.

2.9.3. Intracellular ROS measurement

To evaluate the protective function of the NGL/T and sEVs-NGL/T hydrogels for PC12 cells against oxidative stress, we performed a range of experiments. PC12 cells were seeded into a 12-well plate and co-cultured with different hydrogels. Subsequently, the culture medium was replaced by peroxidative medium containing 100-μM H_2O_2 for 24 h. Following peroxidative culture, the ROS levels in PC12 cells in the different hydrogels were detected using an ROS assay kit (Beijing Solarbio Science & Technology Co., Ltd., Beijing, China) in accordance with the manufacturer's protocols. The production of cellular ROS was measured using dichlorodihydrofluorescein diacetate (DCFH-DA), a nonfluorescent, cell-permeating compound. Samples were observed by fluorescence microscopy (Olympus, Tokyo, Japan) and relative fluorescence was analyzed by Image J (NIH, USA) and GraphPad Prism 8.0 (GraphPad Software, San Diego, CA, USA).

2.10. Generating an animal model of SCI and treatment

Animal experiments were reviewed and approved by the Lab Animal Care and Use Committee of Jiangsu University. All surgical procedures were performed under a sterile environment. Female Sprague–Dawley rats, purchased from the experimental animal center of Jiangsu University, aged 7–8 weeks and weighing 200–220 g at the time of surgery, were used as the SIC model. All animals were maintained under specific pathogen-free conditions and housed under suitable environmental conditions (temperature 24–26 °C, humidity 50%, 12-h light/dark cycle) with sufficient access to food and water. A total of 24 adult Sprague–Dawley rats were randomly divided into the following four groups: sham (n = 6), SCI (n = 6), NGL/T (n = 6), and sEVs-NGL/T (n = 6). The SCI model was prepared *via* complete transection of the spinal cord, as previously described [22]. After weighing, the rats were anesthetized with 10% chloral hydrate (3 mL/kg) and placed in the prone position on an operating table. Fur was removed from the back; after the skin was cut, the muscle was separated for laminectomy to expose the T9–10 segment. The spinal cord was then transected to create a gap of 2.0 ± 0.5 mm. Following precise hemostasis, the different hydrogels were implanted into the lesion gap, ensuring a tight fit. Different treatment strategies were then implemented at the site of injury. Rats receiving laminectomy but no spinal cord transection were prepared as a sham group. Finally, the muscle and skin were sutured. For postsurgical care, penicillin was used for the first 10 days after surgery to prevent infection. The rats received manual bladder massage twice daily until reflexive bladder control was restored.

2.11. Locomotor function investigation

We evaluated motor function in the hind limbs each week after surgery until the end of the experiment. Animals were allowed to walk freely in an open field, and the 21-point Beattie–Beattie–Bresnahan (BBB) locomotion test was conducted by blinded observers over 5 min for each animal. The results were analyzed with GraphPad Prism software.

2.12. The preparation of tissue samples

Animals were sacrificed on day seven for the detection of lipid peroxidation-derived 4-hydroxynonenal (4-HNE) and oxidative DNA damage 8-hydroxy-2′- deoxyguanosine (8-OHdG) levels in the spinal cord tissues and at day 56 for other examinations. The animals were sacrificed by transcardial perfusion of isotonic physiological saline followed by 4% PFA under deep anesthesia. We then dissected the spinal cord (total length: 1.5 cm) encompassing the lesion site. The spinal cord samples were then processed according to the requirements of the corresponding experiments. We also harvested a range of other tissues, including heart, liver, spleen, lung, kidney, and bladder.

2.13. Immunofluorescence staining

Spinal cord tissues were fixed in 4% PFA and processed into 4-μm paraffin sections. The prepared spinal cord slides were then incubated with specific primary antibodies for neurofilament (NF) (Abcam), glial fibrillary acidic protein (GFAP) (Boster Biological Technology, Pleasanton, CA, USA), choline acetyl transferase (ChAT) (Omnimabs, Alambra, CA, USA), 4-HNE (Boster Biological Technology) and 8-OHdG (Boster Biological Technology) overnight at 4 °C. The following morning, the sections were washed and then incubated with Alexa Fluor 555-conjugated donkey anti-mouse IgG (Invitrogen, Waltham, MA, USA) and/or FITC-conjugated goat anti-rabbit IgG (ABclonal, Wuhan, China) secondary antibodies at 37 °C for 1 h. Cell nuclei were counterstained with Hoechst 33342 (1:300; Sigma-Aldrich). The samples were then analyzed by fluorescent microscopy (Nikon, Tokyo, Japan). Image J (NIH, USA) was used for quantitative analysis.

2.14. H&E staining and cavity measurement

To detect the extent of SCI, assess tissue morphology, and determine the site of injury, the spinal cord tissues were fixed in 4% PFA, gradually dehydrated, embedded in paraffin, cut into 5-μm sections, and then stained with Mayer's Hematoxylin and Eosin (H&E). H&E sections were examined to measure the volume of the cavity at the site of SCI. Any necrotic tissue within the cavities was counted as part of the lesion. The areas identified in individual sections were measured using Image J (NIH, USA).

2.15. Masson's trichrome staining

Masson's trichrome staining was conducted using a Masson's Trichrome Stain Kit (Beijing Solarbio Science & Technology Co., Ltd.) in accordance with the manufacturer's protocols. Masson's staining was used for image analysis; analysis was performed with Image-ProPlus 6.0 software (Media Cybernetics Inc., Rockville, MD, USA).

2.16. Cytokine analysis

On the 7th day after surgery, we collected serum samples from each group of rats. Then, we used enzyme-linked immunosorbent assay (ELISA) kits (MultiSciences, Hangzhou, China) to determine the expression levels of TNF-α, IL-1β and IL-6 in the serum of experimental animals; the assays were carried out in accordance with the manufacturer's instructions. Absorbance was measured at a wavelength of 450 nm using a microplate reader.

2.17. Statistical analysis

Data analysis was performed using GraphPad Prism software. The results are presented as mean ± standard deviation (SD). The unpaired Student's t-test was used to compare data between two groups, while one-way analysis of variance (ANOVA) was used to compare multiple groups. *P*-values < 0.05 were considered statistically significant.

3. Results

3.1. Identification and characterization of hucMSCs and hucMSCs-sEVs

HucMSCs were successfully isolated and purified, as described above. The morphology of the HucMSCs revealed a spindle-like shape when viewed microscopically (Fig. 1D). Analysis of the immunophenotypic profile of hucMSCs by flow cytometry revealed that the cells expressed typical MSC surface markers, including CD73 (99.24%), CD29 (99.38%) and CD105 (98.34%), and they showed low expression levels of the B lymphocyte surface markers CD14 (0.87%), CD11 (0.83%), and CD45 (0.49%) (Fig. 1A).

To evaluate the multi-lineage differentiation potential of hucMSCs, we induced such cells to differentiate into adipogenic and osteogenic cells by culturing in adipogenic or osteogenic induction media. Oil-Red-O staining revealed numerous lipid droplets in the cytoplasm of HucMSCs (Fig. 1B), and the cells were positive for alkaline phosphatase (Fig. 1C). These results indicated that hucMSCs showed multi-lineage differentiation. These data suggest that the isolated and expanded hucMSCs exhibited the traits of MSCs. Furthermore, we successfully isolated sEVs from hucMSCs and identified their characteristics using various experiments. TEM, NTA, and Western blot assays were used to identify the morphology; particle sizes, distributions, and diameters; and expression levels of surface markers, respectively. TEM and NTA revealed that sEVs had a spherical shape with an obvious bilayer membrane structure (Fig. 1E); their diameters were approximately 40–150 nm (Fig. 1F). In addition, Western blot analysis indicated that sEV-specific markers (CD81, Alix, and tumor susceptibility gene 101) were expressed on sEVs and not on hucMSCs and that sEVs did not express calnexin (Fig. 1G). In summary, these results confirmed that sEVs had been successfully isolated from hucMSCs.

3.2. Characterization of NGL/T and sEVs-NGL/T hydrogels

SEM images (Fig. 2A and B) revealed a reticular porous structure of the NGL and NGL/T hydrogels. As shown, the TA-treated NGL/T hydrogel had a denser microscopic aperture than the NGL hydrogel. Fig. 2C shows the degradation ratio of the NGL/T hydrogel during incubation on day 70. The degradation rate was small in the first month; this was conducive to providing mechanical support for the damaged tissue. The swelling behavior of the NGL/T hydrogel is presented in Fig. 2D. The swelling equilibrium was reached in 48 h, and the overall

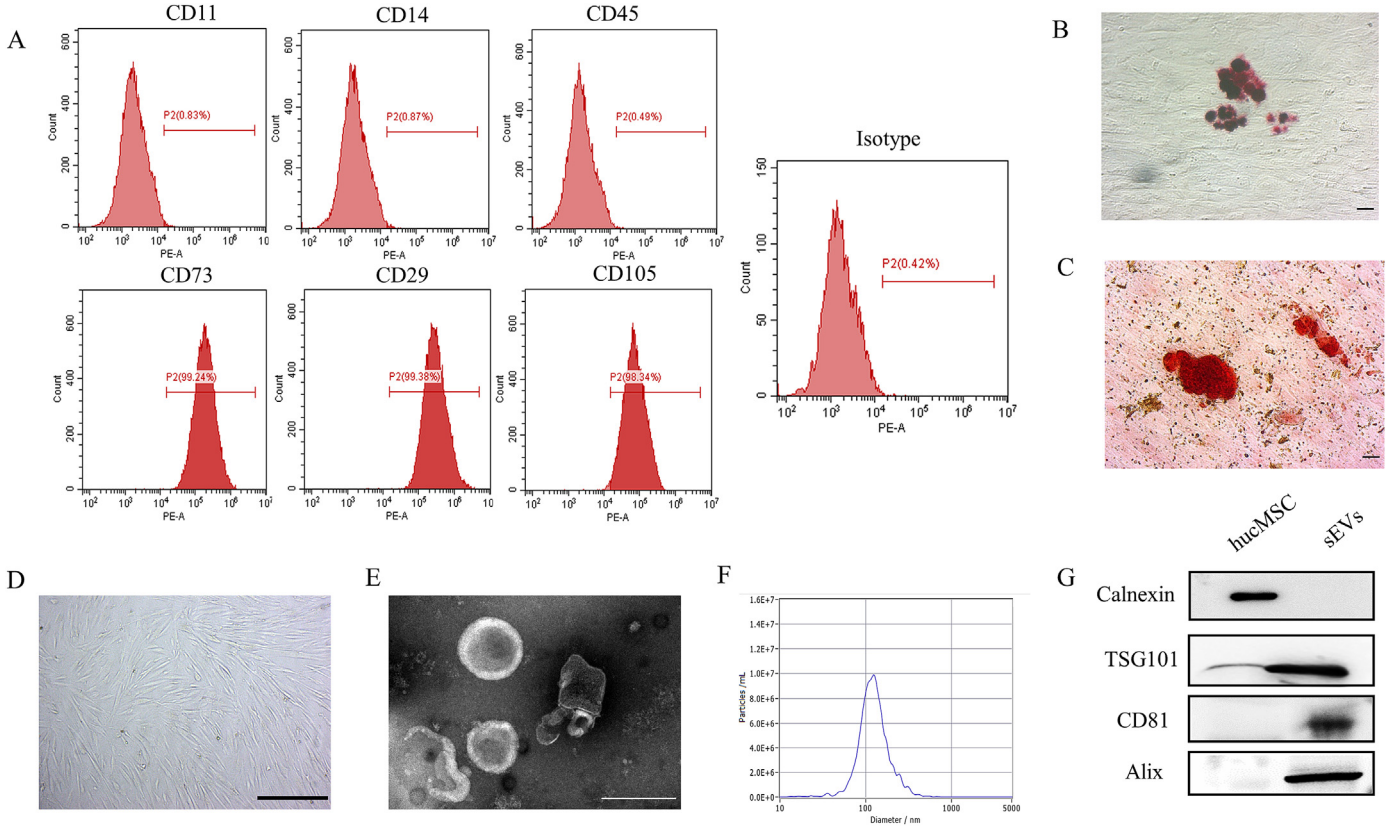

Fig. 1. Identification and characterization of hucMSCs and hucMSCs-sEVs. (A) Flow cytometry analyses of various phenotypic markers for hucMSCs. (B) Stem cell induced differentiation into adipocytes (100×) (C) Stem cell induced differentiation into osteocytes (100×). (D) Morphological identification of hucMSCs (40×). (E) Morphology of sEVs revealed by TEM. Scale bar: 200 nm. (F) Particle size distribution as measured by NTA. (G) Expression of sEVs marker proteins as detected by Western blot analysis.

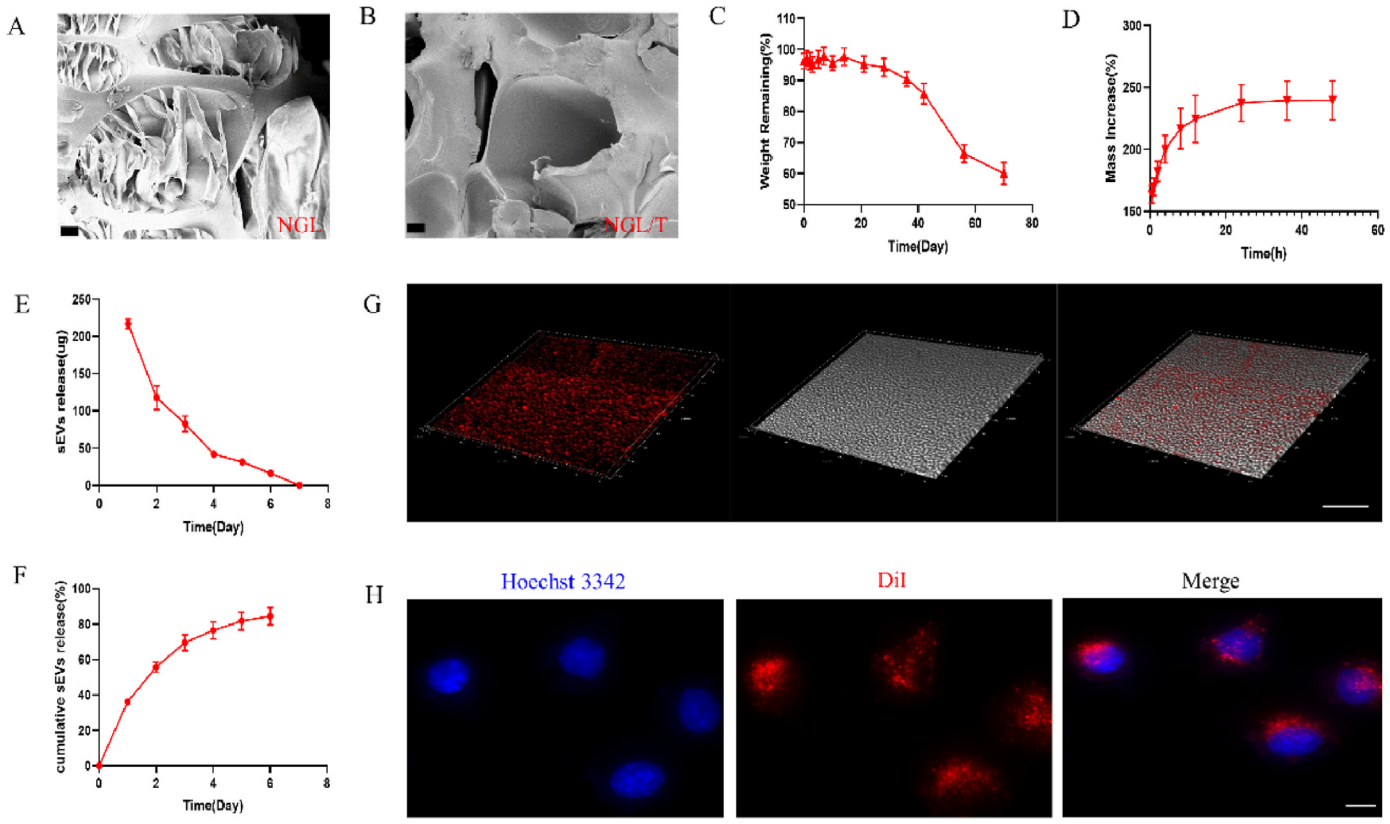

Fig. 2. Characterization of NGL/T and sEVs-NGL/T hydrogels. (A, B) Scanning electron micrographs of NGL (A) and NGL/T (B) hydrogels. Scale bar: 20 μm. (C) Degradation ratio of the NGL/T hydrogels. (D) Swelling ratio of the NGL/T hydrogels in PBS (pH 7.2) at 37 °C. (E) The daily sEV release curve for NGL/T hydrogel (n = 3). (F) Cumulative release profile of sEVs from NGL/T hydrogel (n = 3). (G) sEVs labelled by DiI (red) in NGL/T hydrogel (z-stack). 3D immunofluorescence images revealed the distribution of sEVs in hydrogel. Scale bar: 10 μm. (H) Immunofluorescence images showing that sEVs released from the hydrogel can by phagocytosed by PC12 cells. Scale bar: 10 μm.

swelling rate was low.

As shown in Fig. 2E and F, sEVs loaded in the hydrogels exhibited continuous release for about a week, and more than 80% of the unobstructed loaded sEVs were released from the NGL/T hydrogel. Moreover, the released sEVs did not exhibit significant aggregation or disruption in structures on both the first and third days of release, thus indicating that the sEVs from the sEVs-NGL/T hydrogels retained their normal size and were not damaged by the hydrogel (Supplementary Figure 1). The sustained release of sEVs loaded in the NGL/T hydrogel further ensured its potential application for effective therapeutic delivery and SCI repair. In addition, to confirm that sEVs were successfully loaded into the NGL/T hydrogel, we labelled hucMSC-derived sEVs with DiI, which were then encapsulated in the NGL/T hydrogel *in vitro*. Subsequently, the DiI-sEVs-NGL/T hydrogel was examined by z-stack scanning using a confocal laser scanning microscope. Immunofluorescence images showed that a significantly larger amount of sEVs had adhered to the porous structure and revealed that these were evenly distributed within the hydrogels (Fig. 2G). To confirm that the sEVs released from sEVs-NGL/T hydrogels could be absorbed by PC12 cells, we used DiI to label the sEVs. As shown in Fig. 2H, sEVs were scattered around the nuclei of PC12 cells, indicating that sEVs released from the hydrogel could be phagocytosed normally by PC12 cells and further exhibit other forms of functionality.

3.3. The effects of NGL/T and sEVs-NGL/T hydrogels with regards to antioxidation and neuroprotection

First, to evaluate the antioxidant activity of the NGL/T hydrogels, we performed a DPPH radical scavenging assay; this is widely used to evaluate the free-radical scavenging ability of antioxidants. As shown in Fig. 3A, the DPPH scavenging rate in the NGL/T group reached 95%, compared to only 3% in the NGL group. Subsequently, the antioxidant effect was further evaluated. As shown in Fig. 3C, to simulate the pathological oxidative microenvironment, H_2O_2 was added into the cell culture medium at a concentration of 100 μM. As shown in Fig. 3D, in comparison with the NGL hydrogel group, the NGL/T and sEVs-NGL/T hydrogels led to a significant reduction in H_2O_2 content. Furthermore, we also investigated the potential protective function of the hydrogels in PC12 cells against the ROS microenvironment. PC12 cells were cultured in the hydrogels under simulated ROS conditions (Fig. 3E). The ROS levels in PC12 cells in the different hydrogel groups were detected by DCFH-DA staining. Fig. 3F shows representative fluorescence images of ROS levels in different groups. Quantitative analysis revealed a significantly lower intracellular ROS level in cells cultured in the NGL/T and sEVs-NGL/T hydrogel when compared to the NGL hydrogel (Fig. 3G). The functional hydrogel was used for further investigation.

3.4. The sEVs-NGL/T hydrogel improved pathology and motor function after SCI

The sEVs-NGL/T hydrogel was used for SCI treatment in a rat model of SCI. The spinal cord was transected to form a gap of 2.0 ± 0.5 mm, and the functional hydrogel was fitted into the gap. The surgical and hydrogel implantation processes are illustrated in Fig. 4A and B. The recovery of motor function was tested by the BBB test. Following serious SCI, rats exhibited almost total paralysis in the SCI group, while the rats treated with the sEVs-NGL/T functional hydrogel achieved effective recovery of the motor function in the hindlimbs, with obvious improvement in the BBB score results when compared with the NGL/T and SCI groups on day 56 post-surgery (Fig. 4C). The NGL/T hydrogel only led to relatively limited improvements in functional recovery. In comparison with the

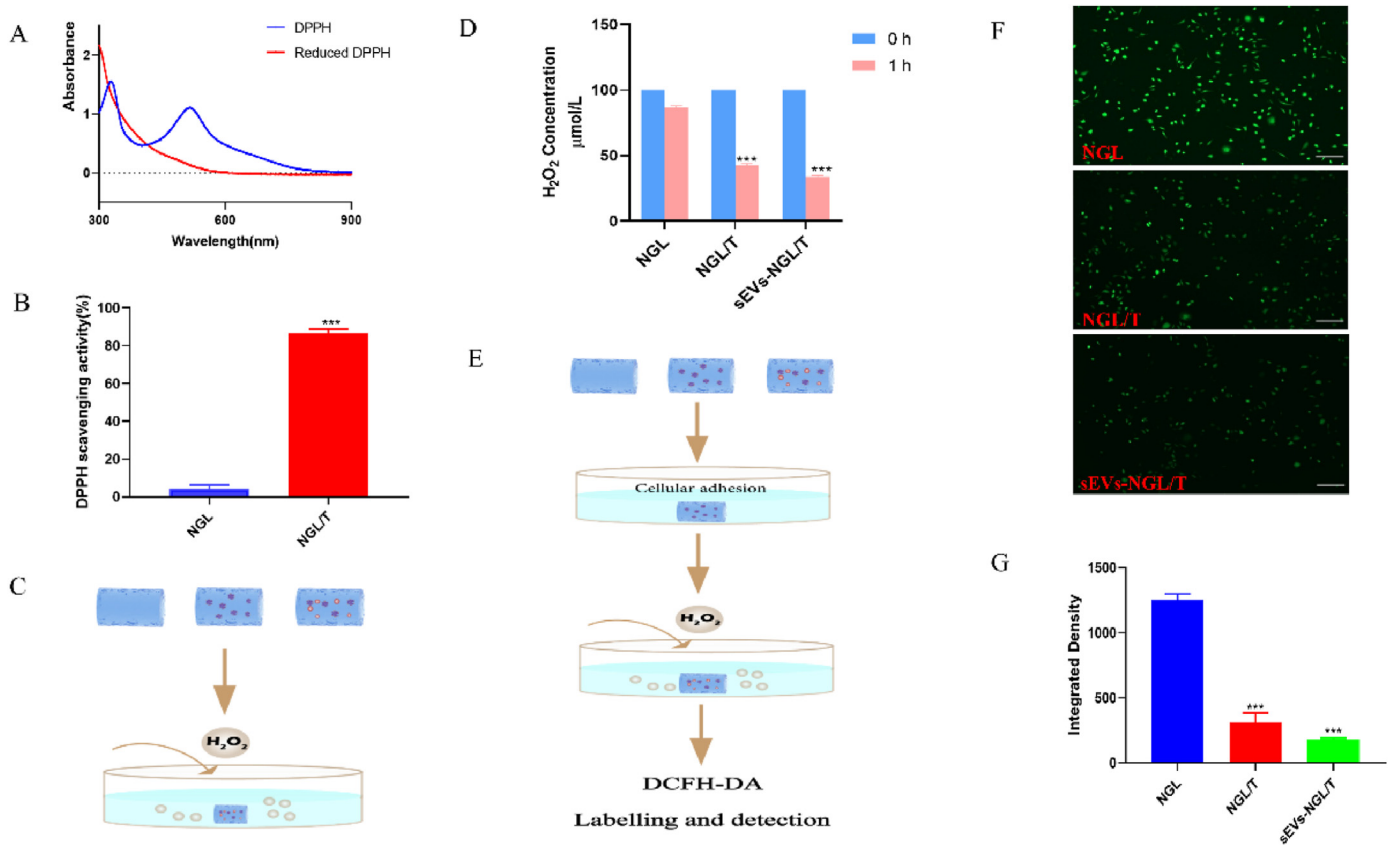

Fig. 3. The effects of sEVs-NGL/T hydrogels with regards to antioxidation and neuroprotection. (A) Absorbance changes of DPPH when exposed to hydrogel. (B) DPPH radical scavenging activities with different hydrogels. (C) Evaluation of the antioxidant effects of NGL/T and sEVs-NGL/T hydrogels *in vitro via* the simulation of a pathological ROS microenvironment in the absence of cells. An initial concentration of H_2O_2 of 100 μM was used in the culture medium in the absence of cells. (D) H_2O_2 levels were detected after incubation with the hydrogels for 1 h. (E) PC12 cells were encapsulated in the hydrogels and allowed to adhere overnight before being exposed to the simulated ROS microenvironment containing 100 μM H_2O_2. (F) Fluorescence images showing ROS levels in different groups. Scale bar: 200 μm. (G) Quantitative results of the intracellular ROS levels of PC12 cells in different groups. Data are presented as mean ± SD, n = 3, $^{***}P < 0.001$ *vs* NGL.

sweeping movements observed in the NGL/T group, we observed a significant improvement in frequent weight-supported steps following sEVs-NGL/T implantation therapy (Fig. 4D). BBB scores showed that the sEVs-NGL/T hydrogel treatment significantly improved functional recovery post-SCI. Furthermore, we analyzed histological morphology and the cavity area in injured spinal cord by H&E staining 56 days after SCI (Fig. 4E). We observed severely damaged tissue and an obvious cystic cavitation in the injured spinal cords 56 days after SCI. As shown in Fig. 4F, the relative area of cystic cavitation in the sEVs-NGL/T group was significantly lower than that in the NGL/T group and SCI group. These results demonstrated that the sEVs-NGL/T hydrogel could effectively improve pathology and motor function after SCI.

3.5. The sEVs-NGL/T hydrogel promoted nerve tissue regeneration after SCI

To further illustrate the anatomical basis of the recovery of locomotor function, we performed immunofluorescence staining of spinal cord tissues in each group to evaluate nerve tissue regeneration on day 56 after surgery. As shown in Fig. 5A, in the SCI group, we observed the aggregation of $GFAP^+$ cells at the edge of the lesion, leaving a poorly repaired cavity with few NFs. After treatment, the density ratio of NF^+ to $GFAP^+$ cells in the sEVs-NGL/T implantation group were significantly reversed. In comparison to the NGL hydrogel, the sEVs-NGL/T hydrogel showed a superior effect in terms of nerve fiber restoration, with a higher neurofilament redistribution and a higher ratio of NF^+ to $GFAP^+$ cells. Moreover, the expression of choline acetyltransferase (ChAT) in spinal cord tissue was also evaluated. Similar results were observed (Fig. 5B); ChAT transmission was effectively restored in the sEVs-NGL/T group. This greater distribution of ChAT was also in accordance with the superior restoration of locomotor function. The results of ChAT staining further demonstrated the regenerative effects of sEVs-NGL/T.

3.6. Antioxidant and anti-inflammatory effects of the sEVs-NGL/T hydrogel in vivo

The antioxidant functions of the sEVs-NGL/T hydrogel were further investigated *in vivo* seven days after implantation. As shown in Fig. 6A and B, both 4-HNE and 8-OHdG were highly expressed in the SCI group, while sEVs-NGL/T treatment markedly reduced the expression of 4-HNE and 8-OHdG. Moreover, NGL/T hydrogel-treated groups were able to suppress oxidative stress well; however, the effect was still lower than in the sEVs-NGL/T treated group. Furthermore, to demonstrate the effect of sEVs-NGL/T hydrogel on the inflammatory reaction, we analyzed the expression of TNF-α, IL-1β, and IL-6 in the serum of experimental rats seven days after hydrogel implantation using ELISA. The levels of TNF-α, IL-1β, and IL-6 were significantly higher in the SCI group; sEVs-NGL/T implantation markedly reduced the expression of these pro-inflammatory cytokines (Fig. 6C, D, E).

3.7. sEVs-NGL/T hydrogel protected the bladder tissue

The recovery of urinary system function depends on the recovery of spinal cord nerve functions; this is also an important indicator for nerve tissue repair effects. The volume (Fig. 7A) and weight (Fig. 7B) of bladders in the SCI groups increased significantly within 56 days of injury

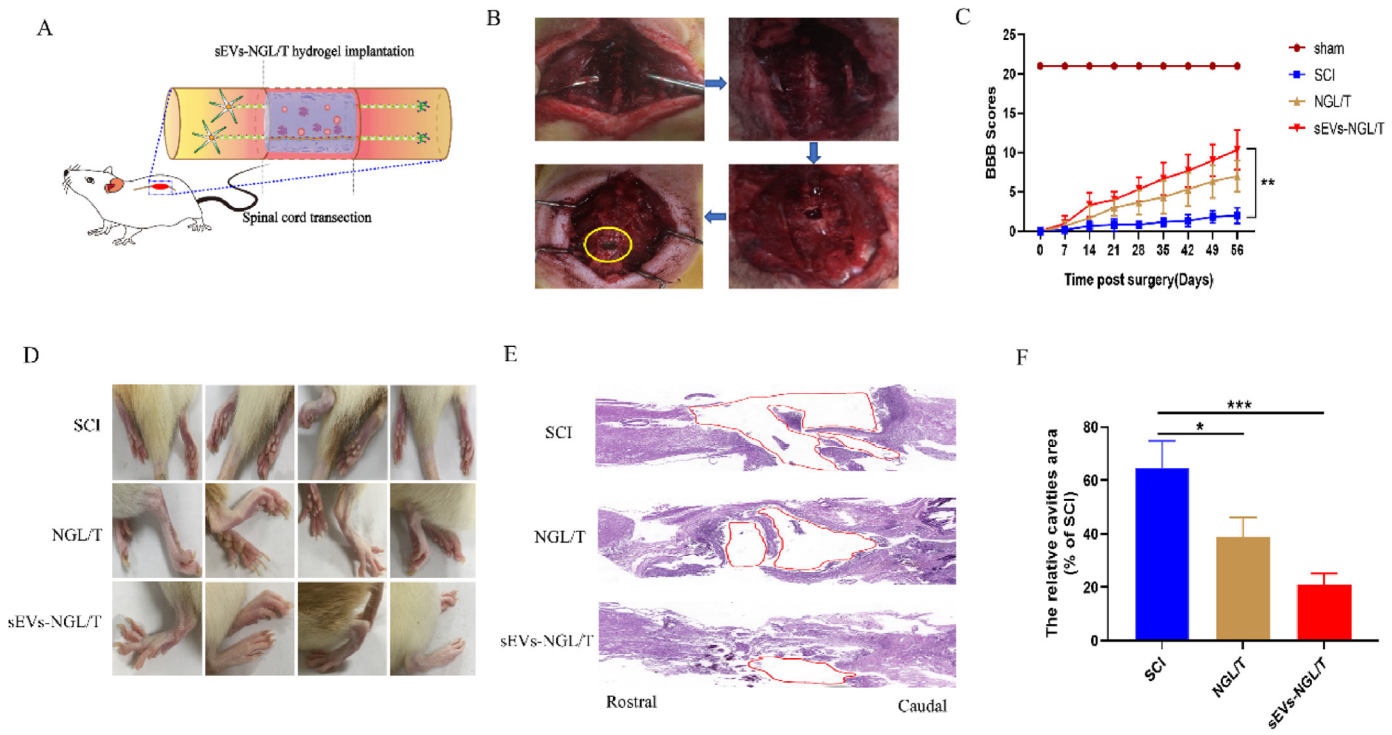

Fig. 4. The sEVs-NGL/T hydrogel enhanced motor function and suppressed cavity formation after SCI. (A) Schematic illustration of spinal cord transection and therapeutic experiments using sEVs-NGL/T hydrogel. (B) Spinal cord transection and hydrogel implantation treatment. (C) Motor functional behavioral recovery of animals in both groups at day 56 post-surgery, as assessed by BBB scores. (D) Typical records of animal walking gaits on day 56 showing hindlimb walking patterns in the different groups. (E) H&E images of spinal cord longitudinal sections at 56 days post-injury. Scale bar: 500 μm. (F) The cavity area was quantified according to the extent of H&E staining. Data are presented as mean ± SD, n = 3, $^{*}P < 0.05$, $^{**}P < 0.01$, $^{***}P < 0.001$ *vs* SCI.

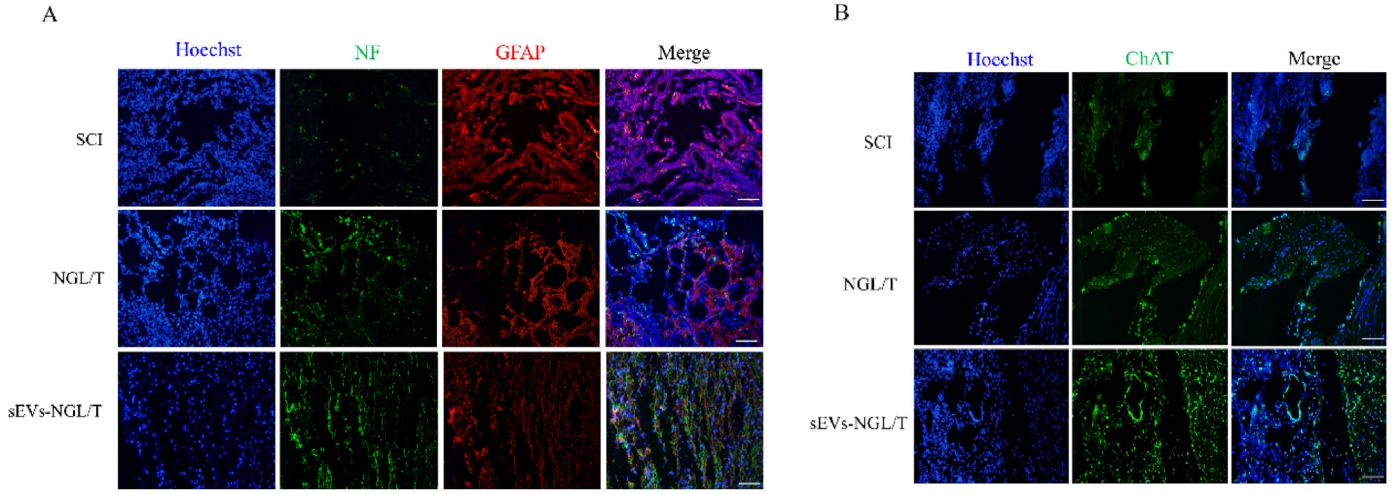

Fig. 5. sEVs-NGL/T hydrogel promoted neurogenesis at the injury site in spinal cord. (A) Representative immunofluorescence images showing the staining of neurofilaments (NFs, green) and glial fibrillary acidic protein (GFAP, red) in the lesion site of spinal cord in different groups. (B) Fluorescent immunostaining of choline acetyl transferase (ChAT) in the lesion site of spinal cord in different groups. The scale bar is 100 μm and applies to all figure sections.

while the urinary bladders of rats in the sEVs-NGL/T treatment group were almost normal. H&E staining showed that there was severe thickening of the bladder wall and disordered muscle bundles in the SCI group, while the sEVs-NGL/T group showed normal morphology of the bladder wall and a regular arrangement of muscle fibers, as observed in the sham group (Fig. 7C). However, the NGL/T group exhibited relatively limited improvement in terms of urinary system function. Masson's staining revealed similar results (Fig. 7D). Compared with the fibrosis and atrophy of muscles in the SCI group, the sEVs-NGL/T group exhibited a healthier tissue condition.

3.8. Biocompatibility and safety evaluation of sEVs-NGL/T hydrogel in vivo and in vitro

To evaluate the biocompatibility of the NGL/T and sEVs-NGL/T hydrogel, we cultured PC12 cells on the surface of NGL/T and sEVs-NGL/T hydrogels for 3 and 7 days, subsequently we used optical microscope to observe the growth morphology of PC12 cells and the results showed that majority of PC12 cells grew well after coculturing with the hydrogels for 7 days (Supplementary Figure 2). Moreover, *in vitro* cytotoxicity of hydrogels against PC12 cells after incubation for 1, 3 and 7

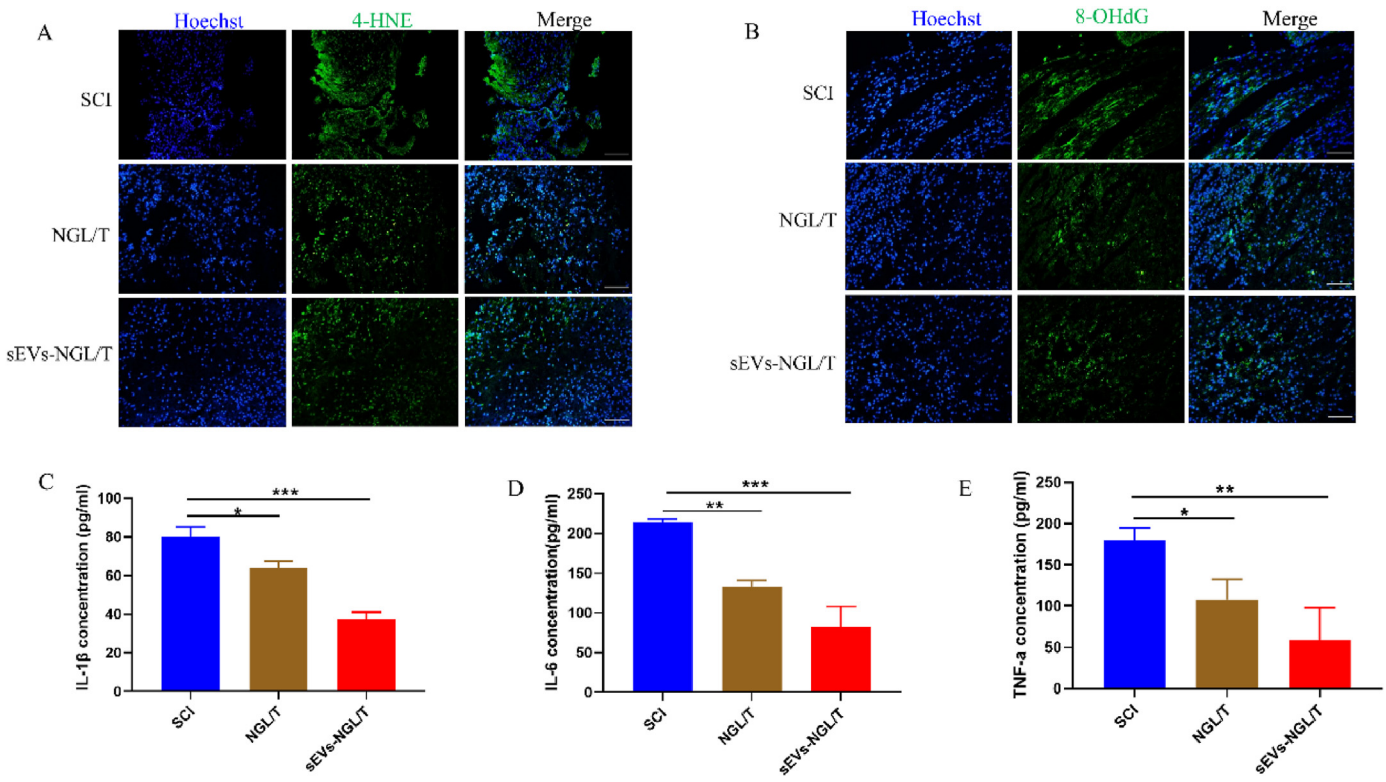

Fig. 6. *In vivo* evaluation of the antioxidant and anti-inflammatory effects of the sEVs-NGL/T hydrogel. (A, B) Detection of the products of the lipid peroxidation-derived 4-hydroxynonenal (4-HNE) and oxidative DNA damage marker 8-hydroxy-2′- deoxyguanosine (8-OHdG) in spinal cord tissues; these confirmed the effective antioxidant and protective functions of the sEVs-NGL/T hydrogel *in vivo*. The scale bar is 100 μm and applies to all figure sections. (C, D, E) ELISA was used to detect inflammatory cytokines (IL-1β, IL-6, and TNF-α). Data are presented as mean ± SD, n = 3, $^{*}P < 0.05$, $^{**}P < 0.01$, and $^{***}P < 0.001$ *vs* SCI.

days was detected by CCK-8 tests. As is shown in Fig. 8A, the results revealed that the cell viability of PC12 cells cultured on sEVs-NGL/T hydrogels was significantly higher than that of the control group and NGL/T group, and exhibited excellent cell proliferation tendency. Furthermore, the cell adhesion and growth morphology were observed by SEM at 7 days. It can be seen from the Fig. 8B that PC12 cells grow well on the surface of NGL/T and sEVs-NGL/T hydrogels and the cells are spindle-shaped with obvious pseudopodia. These results demonstrate that the sEVs-NGL/T hydrogel has good biocompatibility with neurons. Finally, we used H&E to stain tissue samples from the major organs (heart, liver, spleen, lungs, and kidney) of each group. There were no obvious changes or any pathological changes in any of the major organs harvested from the NGL/T and sEVs-NGL/T groups after the 56-day treatment (Fig. 8C), thus further confirming the biocompatibility and safety of this treatment. Furthermore, the mechanism of sEVs-NGL/T hydrogel therapy promoting SCI repair was illustrated in Fig. 9.

4. Discussion

The combination of tissue engineering technology and stem cell-derived sEVs has been widely applied in the repair of tissue damage [23,24]. In this study, we developed a novel hydrogel with antioxidant and anti-inflammatory capabilities that can antagonize the adverse effects of SCI and facilitate tissue repair. Firstly, we successfully isolated and purified HucMSCs and confirmed their potential for multi-lineage differentiation by performing adipogenic and osteogenic induction experiments. Moreover, the immunophenotypic profile of hucMSCs was also demonstrated by flow cytometry using typical MSC surface markers. The results indicated that the isolated and expanded hucMSCs possessed traits that were characteristic of MSCs. After harvesting hucMSCs, we then isolated sEVs. The morphology and particle size distributions of sEVs were analyzed using TEM and NTA. In addition, we detected the expression of specific sEV markers by Western blot. Collectively, our data suggested that sEVs had been successfully isolated from hucMSCs. We also treated NGL hydrogels with TA to establish a functional hydrogel scaffold (NGL/T hydrogel) to enhance antioxidant and anti-inflammatory abilities. We testified the reticular porous structure of NGL and NGL/T hydrogels and confirmed that the NGL/T hydrogel had a denser microscopic aperture than the NGL hydrogel. These data indicated that the size of the pores (100–200 nm) was suitable for cell proliferation and nutrient transmission [25]. This NGL/T hydrogel degraded slowly and provided a good framework with sufficient mechanical support for spinal cord regeneration. We found that the degradation rate was small in the first month, which was conducive to providing mechanical support for the damaged tissue and gradually degraded over the following month, thus ensuring sustained released and therapeutic effects of sEVs. In addition, the swelling rate was small, therefore avoiding excessive swelling that can compress the surrounding tissue after implantation. Moreover, the NGL/T hydrogel was combined with sEVs and retained sustained release capability about one week. By performing *in vitro* experiments, we also showed that sEVs could be phagocytized by PC12 cells, a widely recognized neural cell line [26].

Critically, the introduction of TA into the NGL/T hydrogel resulted in a significantly increased effect on the ability to scavenge DPPH radicals, thus demonstrating an increased antioxidant capacity of the hydrogel [27]. Then, we evaluated the antioxidant function of the NGL/T hydrogel by detecting the concentration of H_2O_2 with a hydrogen peroxide assay kit *in vitro*. Since H_2O_2 could react with FBS proteins from the cell culture medium, the H_2O_2 concentration in the NGL hydrogel group also decreased to a certain extent [28]. However, compared to the NGL hydrogel group, both NGL/T and sEVs-NGL/T hydrogels indicated an increased antioxidant function. Furthermore, we demonstrated the protective function of the NGL/T and sEVs-NGL/T hydrogels in PC12 cells against ROS using DCFH-DA labelling and detection experiments [29].

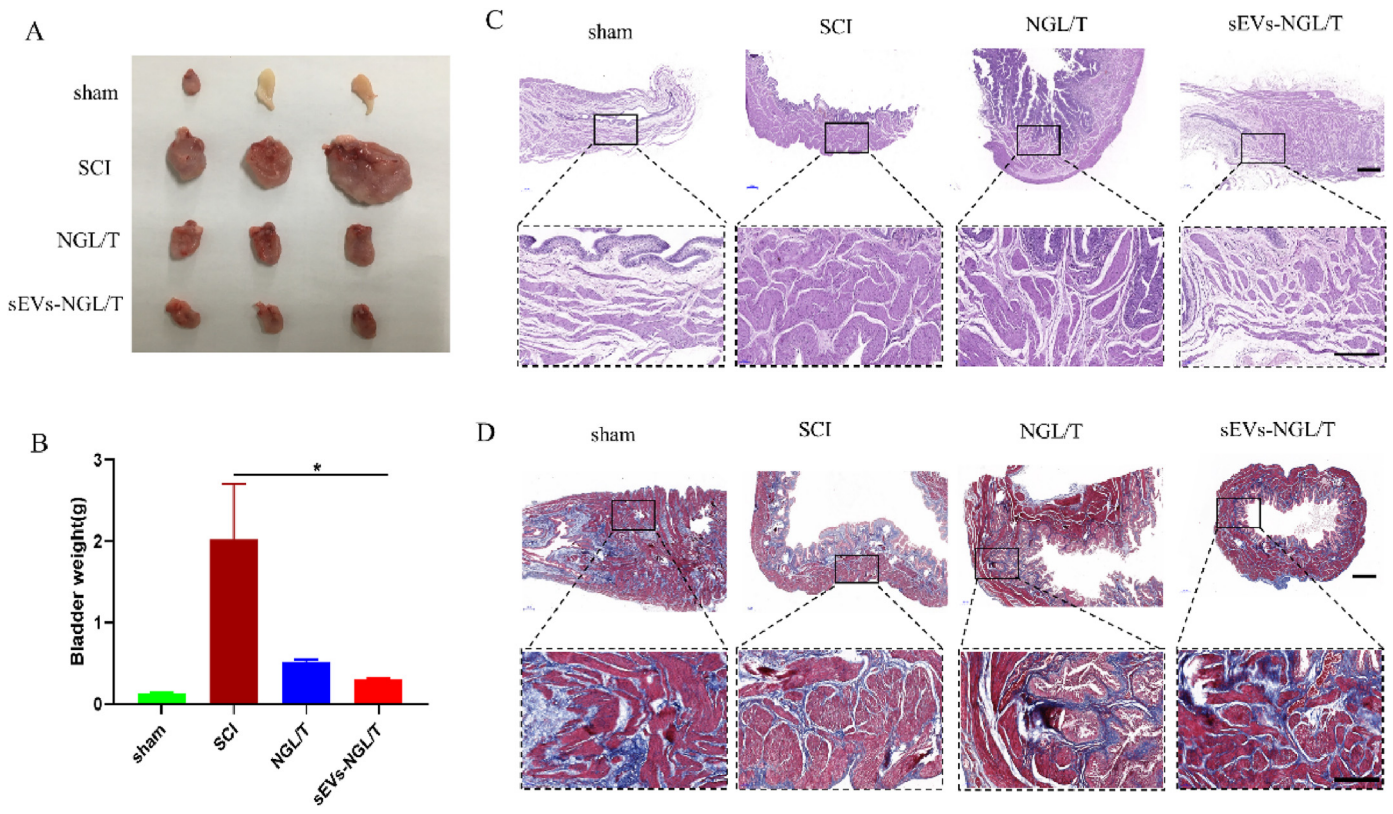

Fig. 7. Examination of bladder tissue at day 56 post-surgery. (A) Analysis of morphological changes in bladders on day 56. (B) Weights of bladders in different groups on day 56. (C) H&E staining of bladder tissues. (D) Masson's staining of bladder tissues. Scale bar: 500 μm (C, D, upper line before magnification) and 100 μm (C, D, lower lines after magnification). Data are presented as mean ± SD, n = 3, $^{*}P < 0.05$ *vs* SCI.

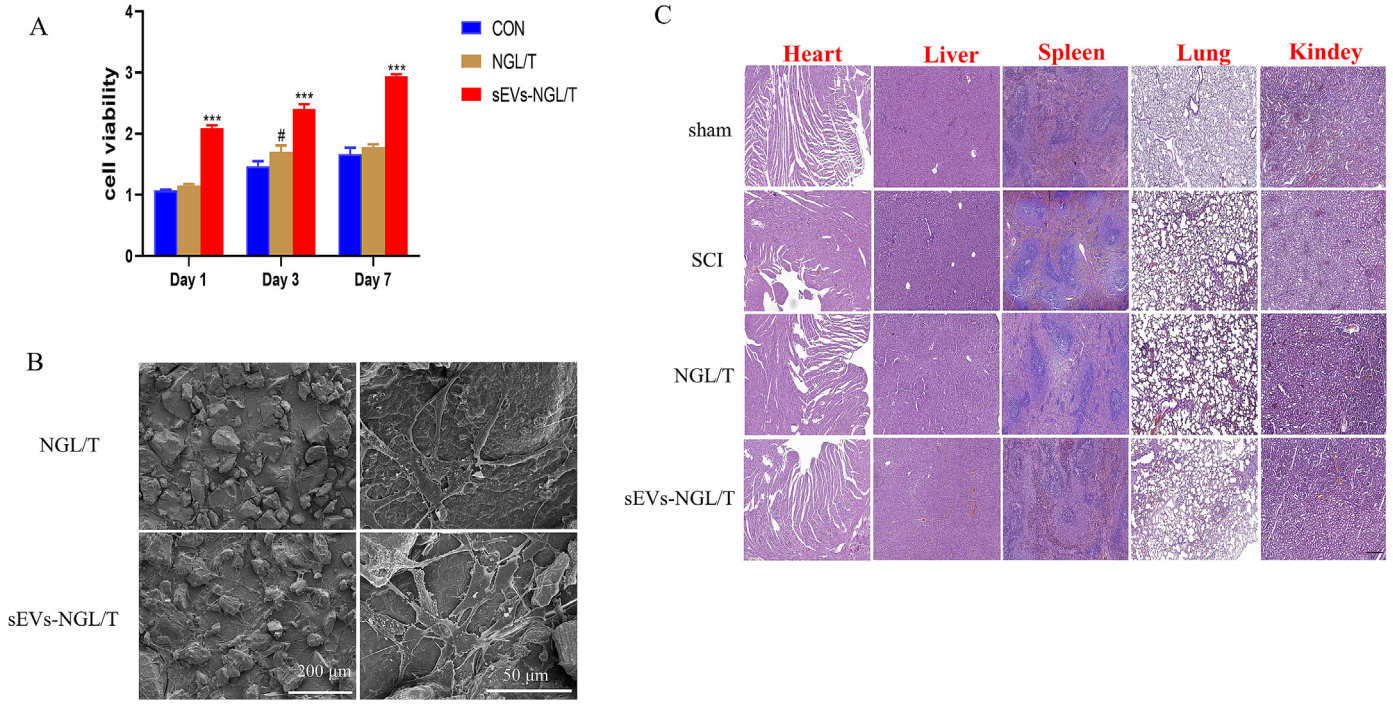

Fig. 8. Biocompatibility and safety evaluation of sEVs-NGL/T hydrogel *in vivo* and *in vitro*. (A) *In vitro* cytotoxicity of hydrogels against PC12 cells after incubation for 1, 3 and 7 days. Data are determined by CCK-8 assays. (B) SEM images of PC12 cells on NGL/T and sEVs-NGL/T hydrogels after incubation for 7 days. (C) HE staining of the heart, liver, spleen, lung, and kidney after the 56 days treatment. The scale bar is 200 μm and applies to all figure sections (C). Data are presented as mean ± SD, n = 4, $^{***}P < 0.001$ *vs* CON.

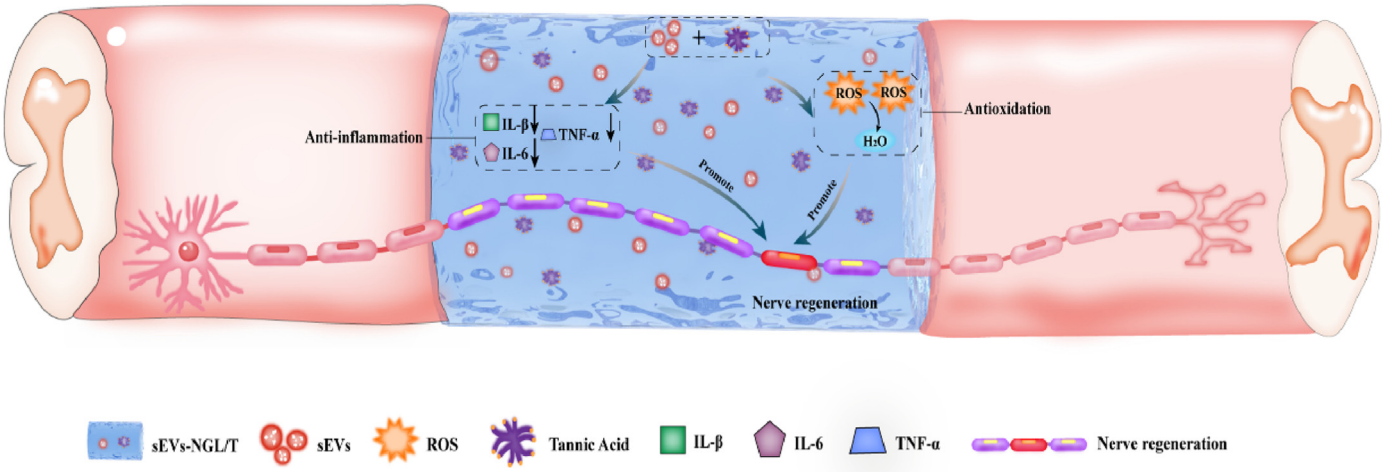

Fig. 9. The mechanism of sEVs-NGL/T hydrogel promoting SCI repair. A sEVs-NGL/T hydrogel was prepared for implantation after spinal cord transection with a lesion gap of 2 ± 0.5 mm. The treatment achieved efficient retention and promoted the sustained release of sEVs, thereby synergistically inducing significant restoration in motor function and urinary tissue preservation by effectively mitigating the ROS microenvironment and inhibiting the release of pro-inflammatory cytokines (TNF-α, IL-6, and IL-1β).

Taken together, these results indicated that the sEVs-NGL/T hydrogel exhibits excellent antioxidant properties *in vitro*.

Next, we verified our *in vitro* results *in vivo* using a well-established rat model of SCI. It is widely accepted that the BBB 21-point scale has high sensitivity and good reliability and validity to evaluate locomotor function in rat models of thoracolumbar SCI [30,31]. BBB scores showed that sEVs-NGL/T hydrogel treatment significantly improved the recovery of locomotor function post-SCI when compared to the SCI and the NGL/T groups. Moreover, the damaged tissue and cystic cavitation were significantly improved in the injured spinal cord after transplanting sEVs-NGL/T when tested 56 days after SCI. The relative area of cystic cavitation in the sEVs-NGL/T group was significantly lower than in the SCI group, indicating the synergistic effects of the NGL/T hydrogel and sEVs. Next, we investigated the anatomical basis of the recovery in locomotor function by analyzing nerve tissue regeneration with immunofluorescence staining. Studies have shown that the formation of glial scars that surround a lesion and isolate a harmful cavity represents the main inhibitor of nerve tissue regeneration after SCI [32]. The main component of glial scars is activated astrocytes; these can be specifically recognized by the marker GFAP [33]. In aggregated astrocytes, the density and distribution of NFs, an indicator of mature neurons that is negatively correlated with the density and distribution of GFAP, can be used to evaluate the extent of nerve tissue regeneration [34]. A more extensive distribution of ChAT, neurotransmitter enzyme found predominantly in cholinergic neurons, has been associated with the superior performance of locomotor functional restoration [35]. We demonstrated that sEVs-NGL/T treatment effectively prevented the excessive accumulation of astrocytes and triggered substantial growth of nerve fibers, thus identifying the important role of sEVs-NGL/T in nerve regeneration after SCI.

We further testified the antioxidant effects of the sEVs-NGL/T hydrogel *in vivo* at 7 days after implantation by analyzing the immunofluorescence staining of 4-HNE and 8-OHdG in the lesion site. 4-HNE and 8-OHdG are products of lipid peroxidation and oxidative DNA damage caused by oxidative stress, respectively, and can cause cell toxicity, affect signal transduction and normal physiological activities, and even lead to cellular apoptosis [36]. Therefore, immunofluorescence staining of 4-HNE and 8-OHdG can represent the severity of oxidative stress in cells, and these molecules are currently recognized as markers for oxidative damage. Our data suggested that oxidative damage was significantly reduced after the implantation of NGL/T and sEVs-NGL/T, likely due to the antioxidant effects of TA in the hydrogels. As shown in previous studies, oxidative stress is the main factor leading to secondary nerve damage and the inhibition of tissue recovery in SCI [37]. After SCI, the dynamic balance of redox reactions in the body is interrupted, mitochondrial function is impaired, and ROS are overproduced, resulting in cell metabolism disorders and dysfunction as well as DNA and protein damage, inducing nerve cell apoptosis and aggravating SCI [38]. Therefore, inhibition of the oxidative stress response after SCI can protect neurons and improve pathology and motor function. It has been reported that treatment with ginseng significantly downregulated oxidative stress by enhancing the antioxidant status in SCI rats and, therefore, facilitated spinal cord functional recovery after injury [39]. In the present study, we demonstrated that oxidative damage was significantly reduced by the sEVs-NGL/T hydrogel. The protective role of sEVs-NGL/T in SCI rats might be attributed to its antioxidant potential. The antioxidant effects of the sEVs-NGL/T hydrogel therefore create a promising therapeutic target for nerve tissue repair after SCI.

SCI is a complex pathophysiological process in which inflammation plays a key role. Inflammatory reactions, including the release of inflammatory cytokines and the infiltration of inflammatory cells, can cause the apoptosis and necrosis of neurons and glial cells, thus hindering the repair process after SCI [40]. Studies have confirmed that pro-inflammatory cytokines, including TNF-α, IL-1β, and IL-6, significantly increased after SCI, promoting inflammatory cell infiltration and further aggravating the injury [41]. Several studies demonstrated that inhibiting the release of pro-inflammatory cytokines was beneficial for the regulation of the injury microenvironment and significantly improved functional recovery after traumatic SCI in rats [42,43]. In the present study, we observed that the implantation of the NGL/T hydrogel inhibited the release of pro-inflammatory cytokines including TNF-α, IL-6, and IL-1β. However, the inhibitory effect in the NGL/T hydrogel group was lower than that in the sEVs-NGL/T treated group, thus implying that a portion of the anti-inflammatory effect was derived from the sEVs [44]. This protective role of sEVs in exerting anti-inflammation is consistent with earlier reports [45]. Moreover, sEVs-NGL/T were able to release sEVs in a sustainable, stable, and controlled manner, thus enhancing the localization of free sEVs at the site of injury in the spinal cord to maintain sustainable anti-inflammatory effects. In addition, the reduced inflammatory reaction was also beneficial for mechanical

compatibility between the spinal cord tissue and the hydrogel implants [46]. Therefore, the positive effects of sEVs-NGL/T on the recovery of function in the spinal cord may be attributed to the inhibition of pro-inflammatory cytokines described above.

Patients with SCI with neurological impairment can readily develop a series of complications, including respiratory complications, neurogenic bladder, spasms, and deep vein thromboses. The dysfunction and pathological changes of the urinary tissues are one of the most common and serious complications, and they can lead to renal failure or even death in severe cases [47]. Therefore, the recovery of bladder function is an important indicator for the evaluation of nerve tissue repair effects. In our study, we demonstrated an effective protective role of sEVs-NGL/T implantation on the recovery of bladder function, thus indicating promising reparative and regeneration effects in the spinal cord.

This study has certain limitations that should be considered. First, the detailed molecular mechanisms underlying the positive effects of sEVs-NGL/T on the recovery of function in the spinal cord have yet to be elucidated. Second, as our sEVs-NGL/T hydrogel is not injectable, the implantation of this hydrogel is associated with an increased likelihood of damage related to surgery. Finally, the release of sEVs from sEVs-NGL/T cannot be controlled accurately *in vivo*, thus reducing the positive effects on the repair of SCI. These issues will be addressed in our future work.

5. Conclusions

In summary, we designed and fabricated a functional hydrogel (sEVs-NGL/T) with excellent anti-oxidative and anti-inflammatory properties, good biocompatibility, and superior sustained release of hucMSC-derived sEVs that can effectively enhance spinal cord repair after SCI. Analysis indicated significant restoration of motor function, nerve tissue repair, and urinary tissue preservation following sEVs-NGL/T therapy. These positive effects may be attributed to effectively mitigating the ROS microenvironment and inhibiting the release of pro-inflammatory cytokines, including TNF-α, IL-6, and IL-1β. The novel sEVs-NGL/T hydrogel provides a promising strategy for the sEV-based therapy of SCI *via* the comprehensive regulation of the pathological microenvironment.

Authorship contribution statement

Zhong Liu: Methodology, Investigation, Validation, Writing-Original draft preparation, Writing-review & editing. **Song Guo:** Conceptualization, Investigation, Writing-original draft, Writing-review & editing. **Lanlan Dong:** Investigation, Data curation, Formal analysis, Validation, Writing-review & editing. **Peipei Wu:** Investigation, Data curation, Formal analysis, Validation. **Xinhua Li:** Investigation, Validation. **Kewei Li:** Investigation, Validation. **Xiang Li**: Conceptualization, Project administration, Supervision. **Hui Qian:** Conceptualization, Project administration, Supervision. **Qiang Fu:** Conceptualization, Funding acquisition, Project administration, Supervision.

Funding

This study was supported by National Natural Science Foundation of China (No. 81971154, 82202694).

Declaration of competing interest

The authors declare the following financial interests/personal relationships which may be considered as potential competing interests: Qiang Fu reports financial support was provided by National Natural Science Foundation of China.

Acknowledgements

We are deeply grateful to Charlesworth author services for their professional editing in written English. We would also like to thank for the support and assistance of all staff in the Key Laboratory of Laboratory Medicine of Jiangsu Province

Appendix A. Supplementary data

Supplementary data to this article can be found online at https://doi.org/10.1016/j.mtbio.2022.100425.

References

[1] P. Assinck, G.J. Duncan, B.J. Hilton, J.R. Plemel, W. Tetzlaff, Cell transplantation therapy for spinal cord injury, Nat. Neurosci. 20 (5) (2017) 637–647.
[2] C. Wutte, B. Klein, J. Becker, O. Mach, S. Panzer, M. Strowitzki, D. Maier, L. Grassner, Earlier decompression (< 8 hours) results in better neurological and functional outcome after traumatic thoracolumbar spinal cord injury, J. Neurotrauma 36 (12) (2019) 2020–2027.
[3] G. Hawryluk, W. Whetstone, R. Saigal, A. Ferguson, J. Talbott, J. Bresnahan, S. Dhall, J. Pan, M. Beattie, G. Manley, Mean arterial blood pressure correlates with neurological recovery after human spinal cord injury: analysis of high frequency physiologic data, J. Neurotrauma 32 (24) (2015) 1958–1967.
[4] M.J. Crowe, J.C. Bresnahan, S.L. Shuman, J.N. Masters, M.S. Crowe, Apoptosis and delayed degeneration after spinal cord injury in rats and monkeys, Nat. Med. 3 (1) (1997) 73–76.
[5] E. Garcia, J. Aguilar-Cevallos, R. Silva-Garcia, A. Ibarra, Cytokine and growth factor Activation in vivo and in vitro after spinal cord injury, Mediat. Inflamm. 2016 (2016), 9476020.
[6] A. Anjum, M. Yazid, M.F. Daud, J. Idris, Y. Lokanathan, Spinal cord injury: pathophysiology, multimolecular interactions, and underlying recovery mechanisms, Int. J. Mol. Sci. 21 (20) (2020) 7533.
[7] D. Edward, Hall, antioxidant therapies for acute spinal cord injury, Neurotherapeutics 8 (2) (2011) 152–167.
[8] C. Ahuja, S. Nori, L. Tetreault, J. Wilson, B. Kwon, J. Harrop, D. Choi, M. Fehlings, Traumatic spinal cord injury-repair and regeneration, Neurosurgery 80 (2017) S9–S22.
[9] Z. Li, F. Wu, D. Xu, Z. Zhi, G. Xu, Inhibition of TREM1 reduces inflammation and oxidative stress after spinal cord injury (SCI) associated with HO-1 expressions, Biomed. Pharmacother. 109 (2019) 2014–2021.
[10] Y.T. Kim, J.M. Caldwell, R.V. Bellamkonda, Nanoparticle-Mediated local delivery of methylprednisolone after spinal cord injury, Biomaterials 30 (13) (2009) 2582–2590.
[11] S. Quideau, D. Deffieux, C. Douat-Casassus, L. Pouységu, Plant polyphenols: chemical properties, biological activities, and synthesis, Angew. Chem. (Int. Ed. Engl.) 50 (3) (2011) 586–621.
[12] X. He, X. Liu, J. Yang, H. Du, C. He, Tannic acid-reinforced methacrylated chitosan/methacrylated silk fibroin hydrogels with multifunctionality for accelerating wound healing, Carbohydr. Polym. 247 (2020), 116689.
[13] Y. Li, M. Chen, J. Yan, W. Zhou, S. Gao, S. Liu, Q. Li, Y. Zheng, Y. Cheng, Q. Guo, Tannic acid/Sr(2+)-coated silk/graphene oxide-based meniscus scaffold with anti-inflammatory and anti-ROS functions for cartilage protection and delaying osteoarthritis, Acta Biomater. 126 (2021) 119–131.
[14] H. Inoue, S. Akiyama, M. Maeda-Yamamoto, A. Nesumi, T. Tanaka, A. Murakami, High-dose green tea polyphenols induce nephrotoxicity in dextran sulfate sodium-induced colitis mice by down-regulation of antioxidant enzymes and heat-shock protein expressions, Cell Stress Chaperones 16 (6) (2011) 653–662.
[15] Q. Wang, Y. He, Y. Zhao, H. Xie, Q. Lin, Z. He, X. Wang, J. Li, H. Zhang, C. Wang, A Thermosensitive heparin-poloxamer hydrogel bridge aFGF to treat spinal cord injury, ACS Appl. Mater. Interfaces 9 (8) (2017) 6725.
[16] C. Zhao, X. Zhou, J. Qiu, D. Xin, D. Wang, Exosomes derived from bone marrow mesenchymal stem cells inhibit complement activation in rats with spinal cord injury, Drug Des. Dev. Ther. 13 (2019) 3693–3704.
[17] J. Kang, Y. Guo, Human umbilical cord mesenchymal stem cells derived exosomes promote neurological function recovery in a rat spinal cord injury model, Neurochem. Res. 47 (6) (2022) 1532–1540.
[18] L. Li, Y. Zhang, J. Mu, J. Chen, C. Zhang, H. Cao, J. Gao, Transplantation of human mesenchymal stem-cell-derived exosomes immobilized in an adhesive hydrogel for effective treatment of spinal cord injury, Nano Lett. 20 (6) (2020) 4298–4305.
[19] P. Romanelli, L. Bieler, P. Heimel, S. Škokić, D. Jakubecova, C. Kreutzer, P. Zaunmair, T. Smolčić, B. Benedetti, E. Rohde, M. Gimona, D. Hercher, M. Dobrivojević Radmilović, S. Couillard-Despres, Enhancing functional recovery through intralesional application of extracellular vesicles in a rat model of traumatic spinal cord injury, Front. Cell. Neurosci. 15 (2021), 795008.
[20] C. Subra, K. Laulagnier, B. Perret, M. Record, Exosome lipidomics unravels lipid sorting at the level of multivesicular bodies, Biochimie 89 (2) (2007) 205–212.
[21] P. Wu, B. Zhang, X. Han, Y. Sun, Z. Sun, L. Li, X. Zhou, Q. Jin, P. Fu, W. Xu, H. Qian, HucMSC exosome-delivered 14-3-3ζ alleviates ultraviolet radiation-induced photodamage via SIRT1 pathway modulation, Aging 13 (8) (2021) 11542–11563.
[22] Y. Zhang, L. Li, J. Mu, J. Chen, S. Feng, J. Gao, Implantation of a functional TEMPO-hydrogel induces recovery from rat spinal cord transection through promoting nerve regeneration and protecting bladder tissue, Biomater. Sci. 8 (6) (2020) 1695–1701.
[23] C. Wang, M. Wang, K. Xia, J. Wang, F. Cheng, K. Shi, L. Ying, C. Yu, H. Xu, S. Xiao, C. Liang, F. Li, B. Lei, Q. Chen, A bioactive injectable self-healing anti-inflammatory

hydrogel with ultralong extracellular vesicles release synergistically enhances motor functional recovery of spinal cord injury, Bioact. Mater. 6 (8) (2021) 2523–2534.
[24] S. Ma, H. Hu, J. Wu, X. Li, X. Ma, Z. Zhao, Z. Liu, C. Wu, B. Zhao, Y. Wang, W. Jing, Functional extracellular matrix hydrogel modified with MSC-derived small extracellular vesicles for chronic wound healing, Cell Prolif (2022), e13196.
[25] H. Hu, L. Dong, Z. Bu, Y. Shen, Z. Liu, miR-23a-3p-abundant small extracellular vesicles released from Gelma/nanoclay hydrogel for cartilage regeneration, J. Extracell. Vesicles 9 (1) (2020), 1778883.
[26] J. Hsu, S.J. Shiue, K.D. Yang, H.S. Shiue, J.K. Cheng, Locally applied stem cell exosome-Scaffold attenuates nerve injury-induced pain in rats, J. Pain Res. 13 (2020) 3257–3268.
[27] İ. Gulcin, Antioxidants and antioxidant methods: an updated overview, Arch. Toxicol. 94 (3) (2020) 651–715.
[28] K.S. Yahya, A.S. Mohammad, Effect of human and bovine serum albumin on kinetic chemiluminescence of Mn (III)-Tetrakis (4-sulfonatophenyl) porphyrin-luminol-hydrogen peroxide system, Sci. World J. 2012 (4909) (2012), 913412.
[29] L. Jing, R. Gao, J. Zhang, D. Zhang, J. Shao, Z. Jia, H. Ma, Norwogonin attenuates hypoxia-induced oxidative stress and apoptosis in PC12 cells, BMC Compl. Med. Ther. 21 (1) (2021) 1–12.
[30] J.T. Ye, F.T. Li, S.L. Huang, J.L. Xue, Y. Aihaiti, H. Wu, R.X. Liu, B. Cheng, Effects of ginsenoside Rb1 on spinal cord ischemia-reperfusion injury in rats, J. Orthop. Surg. Res. 14 (1) (2019) 259.
[31] J. Cheng, Z. Chen, C. Liu, M. Zhong, S. Wang, Y. Sun, H. Wen, T. Shu, Bone mesenchymal stem cell-derived exosome-loaded injectable hydrogel for minimally invasive treatment of spinal cord injury, Nanomedicine (Lond.) 16 (18) (2021) 1567–1579.
[32] Y. Zhang, S. Yang, C. Liu, X. Han, X. Gu, S. Zhou, Deciphering glial scar after spinal cord injury, Burns Trauma 9 (2021) tkab035.
[33] S. Zhang, M. Wu, C. Peng, G. Zhao, R. Gu, GFAP expression in injured astrocytes in rats, Exp. Ther. Med. 14 (3) (2017) 1905–1908.
[34] J.R. Mclean, T.R. Sanelli, C. Leystra-Lantz, B.P. He, M.J. Strong, Temporal profiles of neuronal degeneration, glial proliferation, and cell death in hNFL(+/+) and NFL(-/-) mice, Glia 52 (1) (2010) 59–69.
[35] B. Brommer, M. He, Z. Zhang, Z. Yang, J.C. Page, J. Su, Y. Zhang, J. Zhu, E. Gouy, J. Tang, P. Williams, W. Dai, Q. Wang, R. Solinsky, B. Chen, Z. He, Improving hindlimb locomotor function by Non-invasive AAV-mediated manipulations of propriospinal neurons in mice with complete spinal cord injury, Nat. Commun. 12 (1) (2021) 781.
[36] Alper Baran, Yavuz Saglam, Ozkaraca Selim, Parlak Mustafa, Kokturk Veysel, Immunofluorescence evaluation of 4-hydroxynonenal and 8-hydroxy2-deoxyguanosine activation in zebrafish (Daino rerio) larvae brain exposed (microinjected) to propyl gallate, Chemosphere: Environ. Toxicol. Risk Assess. 183 (Sep.) (2017) 252–256.
[37] Z. Jia, H. Zhu, J. Li, X. Wang, H. Misra, Y. Li, Oxidative stress in spinal cord injury and antioxidant-based intervention, Spinal Cord 50 (4) (2012) 264–274.
[38] R. Thanan, S. Oikawa, Y. Hiraku, S. Ohnishi, N. Ma, S. Pinlaor, P. Yongvanit, S. Kawanishi, M. Murata, Oxidative stress and its significant roles in neurodegenerative diseases and cancer, Int. J. Mol. Sci. 16 (1) (2014) 193–217.
[39] W. Wang, H. Shen, J.J. Xie, J. Ling, H. Lu, Neuroprotective effect of ginseng against spinal cord injury induced oxidative stress and inflammatory responses, Int. J. Clin. Exp. Med. 8 (3) (2015) 3514–3521.
[40] D. Dutta, N. Khan, J. Wu, S.M. Jay, Extracellular vesicles as an emerging frontier in spinal cord injury pathobiology and therapy, Trends Neurosci. 44 (6) (2021) 492–506.
[41] Y. Zhu, H. Zhu, Z. Wang, F. Gao, J. Wang, W. Zhang, Wogonoside alleviates inflammation induced by traumatic spinal cord injury by suppressing NF-κB and NLRP3 inflammasome activation, Exp. Ther. Med. 14 (4) (2017) 3304–3308.
[42] S. David, A. Kroner, Repertoire of microglial and macrophage responses after spinal cord injury, Nat. Rev. Neurosci. 12 (7) (2011) 388–399.
[43] J.H. Huang, X.M. Yin, Y. Xu, C.C. Xu, X. Lin, F.B. Ye, Y. Cao, F.Y. Lin, Systemic administration of exosomes released from mesenchymal stromal cells attenuates apoptosis, inflammation, and promotes angiogenesis after spinal cord injury in rats, J. Neurotrauma 34 (24) (2017) 3388–3396.
[44] B. Zhang, F. Lin, J. Dong, J. Liu, J. Xu, Peripheral macrophage-derived exosomes promote repair after spinal cord injury by inducing local anti-inflammatory type microglial polarization via increasing autophagy, Int. J. Biol. Sci. 17 (5) (2021) 1339–1352.
[45] G. Sun, G. Li, D. Li, W. Huang, R. Zhang, H. Zhang, Y. Duan, B. Wang, hucMSC derived exosomes promote functional recovery in spinal cord injury mice via attenuating inflammation, Mater. Sci. Eng. C Mater. Biol. Appl. 89 (2018) 194–204.
[46] Y. Iwasaki, S.I. Sawada, K. Ishihara, G. Khang, B.L. Hai, Reduction of surface-induced inflammatory reaction on PLGA/MPC polymer blend, Biomaterials 23 (18) (2002) 3897–3903.
[47] W.A. Taweel, R. Seyam, Neurogenic bladder in spinal cord injury patients, Res. Rep. Urol. 7 (2015) 85–99.